Journal of Solid State Chemistry **144,** 354–360 (1999)
Article ID jssc.1999.8165, available online at http://www.idealibrary.com on IDEAL®

Dependence of ac Conductivity on Temperature and Frequency in Cerium(III) Nitrate Crystal

Riki Kawashima, Hironori Takahasi,[1] and Hiroshi Isoda

Department of Materials Science and Engineering, Muroran Institute of Technology, Muroran 050, Japan

Received August 20, 1998; in revised form January 14, 1999; accepted January 15, 1999

Ac conductivity spectra from 20 Hz to 1 MHz along the *c* axis of a cerium(III) nitrate hexahydrate $Ce(NO_3)_3 \cdot 6H_2O$ crystal and perpendicular to it were measured at temperatures from room temperature (RT) to 10 K. A metastable phase was found from RT to about 223 K. A peak was found in the conductivity near 130 K perpendicular to the *c* axis. The behavior of the conductivity is dependent on the crystal direction but independent of the measuring run. © 1999 Academic Press

INTRODUCTION

The properties of cerium compounds are of considerable interest because hybridization of the *f* electrons with electrons in the conduction band gives rise to a variety of interesting phenomena such as the valence instabilities (1) and the big fermion (2).

Rare-earth nitrate crystals are dielectric compounds at room temperature having space group symmetry $P\bar{1}$ (3). Metastable phenomena, dependent on the samples and measuring runs, have been identified in successive measurements of the electric properties over the temperature range $\sim 228\ \mathrm{K} < T < \sim 283\ \mathrm{K}$, for numerous rare earth nitrate crystals (La (4), Nd (5), Sm (6), Eu (7), Gd (8), Tb (9), Er (10), and Yb (11)).

An aging effect of the electric properties has been reported for several crystals (4, 9, 11). Nonlinear deterministic properties with a memory effect in the metastable phenomena have been studied by analyzing the variation of the conductivity with time and temperature (12). Characteristic magnetic behaviors dependent on the rare-earth ions have been observed (13) in measurements made on at temperatures in the range 4.2 to 300 K with a SQUID detector system.

In this paper, we report ac conductivity spectra ($20 \le \nu \le 10^6$ H) of $Ce(NO_3)_3 \cdot 6H_2O$ measured at temperatures ranging from 10 K to RT along the *c* axis and perpendicular to it. We found no previous reports of the material properties of the crystal (14). The dynamical property is characterized by exponents of the frequency power law found in the ac conductivity spectra. The properties and mechanisms of the characteristic phenomena are discussed.

EXPERIMENTAL

The crystals used in the present study were grown in a cerium(III) nitrate aqueous solution by decreasing the temperature from 308.25 to 307.25 K over a 590 h interval. The habit of the crystals is consistent with those of the rare-earth nitrate hexahydrates ($R(NO_3)_3 \cdot 6H_2O$), the chemical properties of which are most stable when compared to those of other crystalline nitrate hydrates $R(NO_3)_3 \cdot nH_2O$. The sample sizes used for the measurements and the aging conditions are given in Table 1, where the aging period is defined as the time elapsed after the mother crystal was grown.

The ac conductivity spectra were measured by using a computer-controlled LCR meter (HP4284A) (NEC PC9801E) with the general purpose interface bus (GPIB) at the sensitivity within $\pm 10^{-11}\ \Omega^{-1}\ \mathrm{cm}^{-1}$. The conductivity spectra were measured in sequential runs by sweeping the frequency from 20 Hz to 1 MHz at fixed temperatures controlled by the computer to within ± 0.1 K.

The copper block was set in a adiabatic stainless-steel holder surrounded in alcohol, where temperature was kept constant at 193.15 K by a chiller (Tokyo Rikakikai Co. Ltd., EC-80). The temperature of the specimen was measured with a copper-constantan thermocouple mounted in the sample cell. The electric properties of the specimen at temperatures from 200 to 10 K were controlled and measured by using the closed cycle refrigerator system (Model CCS-250, Janis Research).

RESULTS

AC Conductivity Spectra in Higher Temperature Region

The real part $\sigma'(T)$ of the complex conductivity σ^* along the *c* axis of $Ce(NO_3)_3 \cdot 6H_2O$ and perpendicular to it at

[1]Present address: Sanken Setubi Co., Ltd., 103 Tokyo.

0022-4596/99 $30.00

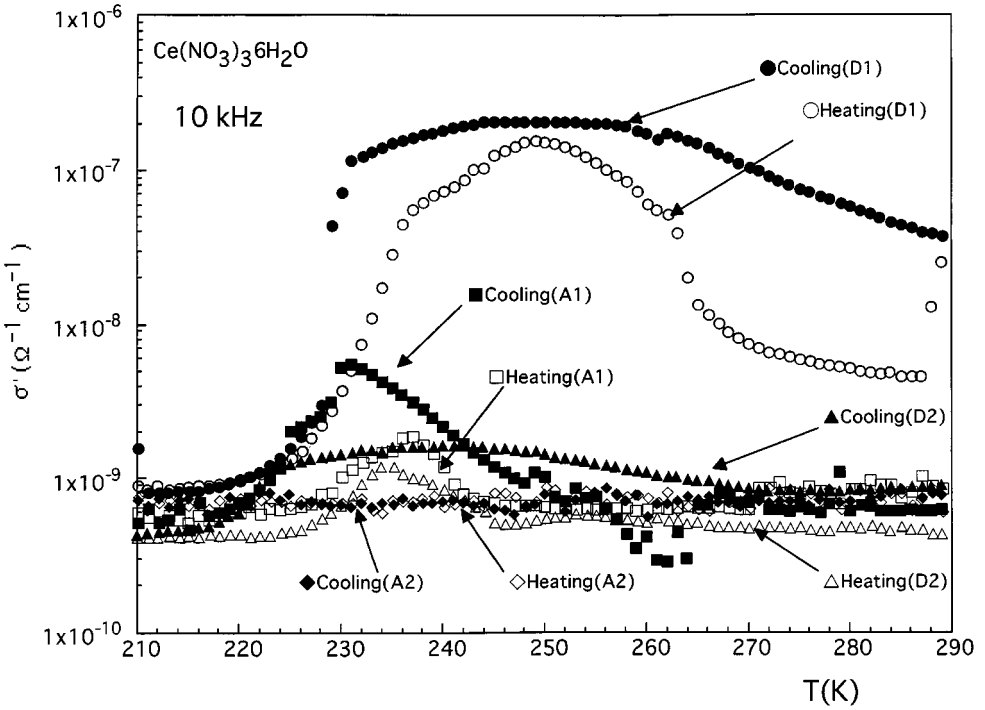

FIG. 1. The real part σ' of the complex conductivity σ^* at 10 kHz in the temperature region from 210 to 290 K, along the c axis of $Ce(NO_3)_3 \cdot 6H_2O$ crystal in cooling (A1) (■) and (A2) (◆) and heating (A1) (□) and (A2) (◇) cycles of double measuring runs, and perpendicular to it in cooling (D1) (●) and (D2) (▲) and heating (D1) (○) and (D2) (△) cycles of double measuring runs.

10 kHz is shown in Fig. 1 at temperatures between 290 and 210 K in cooling and heating cycles (measuring runs, A and D) in a semi-logarithmic scale and is given in Table 1. As seen from Fig. 1, $\sigma'(T)$ for both the cooling and heating cycles of measuring run (1) show appreciable temperature variation with thermal hysteresis in the region between room temperature and ~ 223 K and anisotropy.

The behavior of $\sigma'(T)$ found in runs (A1) and (D1) can be attributed to the existence of a metastable cerium nitrate phase. On the other hand, the behavior apparent in subsequent measuring runs (A2) and (D2) in this temperature range corresponds to that of a stable phase.

The experimental results have been reproduced on several $Ce(NO_3)_3 \cdot 6H_2O$ samples. The detailed behavior that we attribute to the metastable phenomena is dependent on the rare-earth ion R^{3+} in $R(NO_3)_3 \cdot 6H_2O$ (4–11).

Figure 2 shows the frequency dependence of $\sigma'(\nu)$ on the logarithmic plane in the range 100 Hz $\leq$ 1 MHz at several temperatures for cooling cycle (A1). As can be seen in Fig. 2, the conductivity spectra show two different power law dependences represented by

$$\sigma'(\nu, T) \propto A\nu^{s_i(T)}, \qquad [1]$$

where $s_i(T)$ $(i = 1,2)$ are frequency exponents at temperature T (15). The values of the frequency power law exponents $s_1(T)$ and $s_2(T)$ are derived from the frequency gradient of $\sigma'(\nu)$ in both the higher and lower frequency regions, $10^5 \leq \nu \leq 10^6$ Hz and $10^2 \leq \nu \leq 10^3$ Hz, respectively.

The frequency exponents $s_1(T)$ and $s_2(T)$ are given as a function of temperature in Figs. 3 and 4 for the spectra $\sigma'(\nu)$ along the c axis and perpendicular to it, respectively. In the metastable phase region for the spectra $\sigma'(\nu)$ along the c axis, $s_1(T)$ decreases from 1.9 to about 1.7, and $s_2(T)$ increases from 0.2 to 0.3 then decreases. In the same region, but perpendicular to the c axis, $s_1(T)$ decreases from 1.9 to ~ 1.2 in run (D1) and from ~ 1.5 to about 1.1 in run (D2). The data in Figs. 3 and 4 show anisotropy and the dynamical properties of the metastable phase. On the other hand, $s_2(T)$ shows a weak temperature dependence between 0 and about 0.3 for the spectra both along the c axis and perpendicular to it at all temperatures in both the metastable and stable phases.

AC Conductivity Spectra in Lower Temperature Region

Figure 5 shows the real part $\sigma'(T)$ of the complex conductivity σ^* taken at 10 kHz along the c axis of $Ce(NO_3)_3 \cdot 6H_2O$ and perpendicular to it at temperatures from 200 to 10 K in cooling and heating (measuring runs, B and C). The measuring conditions are given in Table 1.

TABLE 1
Sizes of Four Samples, A, B, C, and D, and the Conditions of Measuring Runs for the Respective Measurements

$Ce(NO_3)_3 6H_2O$ sample, direction, sample size area (cm^2), and thickness (cm)	Run number	Temperature range	Aging periods (hours) from crystal growth
A	Cooling (A1)	Cooling from 293.15 to 210.15 K	77
along c axis 0.274 cm^2, 0.071 cm	Heating (A1)	heating from 210.15 to 293.15 K	196
	Cooling (A2)	Cooling from 293.15 to 208.15 K	277
	Heating (A2)	heating from 208.15 to 293.15 K	386
B	Cooling (B1)	Cooling from 200 to 10 K	543
along c axis 0.435 cm^2, 0.035 cm	Heating (B1)	heating from 10 to 200 K	664
	Cooling (B2)	Cooling from 200 to 10 K	846
	Heating (B2)	heating from 10 to 200 K	971
	Cooling (C1)	Cooling from 200 to 10 K	13425
C	Heating (C1)	heating from 10 to 200 K	13546
perpendicular to c axis	Cooling (C2)	Cooling from 200 to 10 K	13673
0.410 cm^2, 0.038 cm	Heating (C2)	heating from 10 to 200 K	13796
	Cooling (D1)	Cooling from 293.15 to 203.15 K	14854
D	Heating (D1)	heating from 203.15 to 293.15 K	14987
perpendicular to c axis	Cooling (D2)	Cooling from 293.15to 203.15 K	15087
0.422 cm^2, 0.089 cm	Heating (D2)	heating from 203.15 to 293.15 K	15184

Note. The aging period is defined as the elapsed time after the mother crystal was grown.

Near 130 K $\sigma'(T)$ shows a noticeable symmetric temperature variation perpendicular to the c axis and a very weak variation along the c axis. The peaks of $\sigma'(T)$ for the lower temperature region in Fig. 5 show independence of the measuring runs, different from those observed in the higher region as given in Fig. 1. Similar anisotropic behavior of $\sigma'(T)$ is found in both the lower and higher temperature regions.

The frequency power law exponents $s_1(T)$ and $s_2(T)$ in both regions are given in Fig. 6 for the spectra $\sigma'(\nu)$

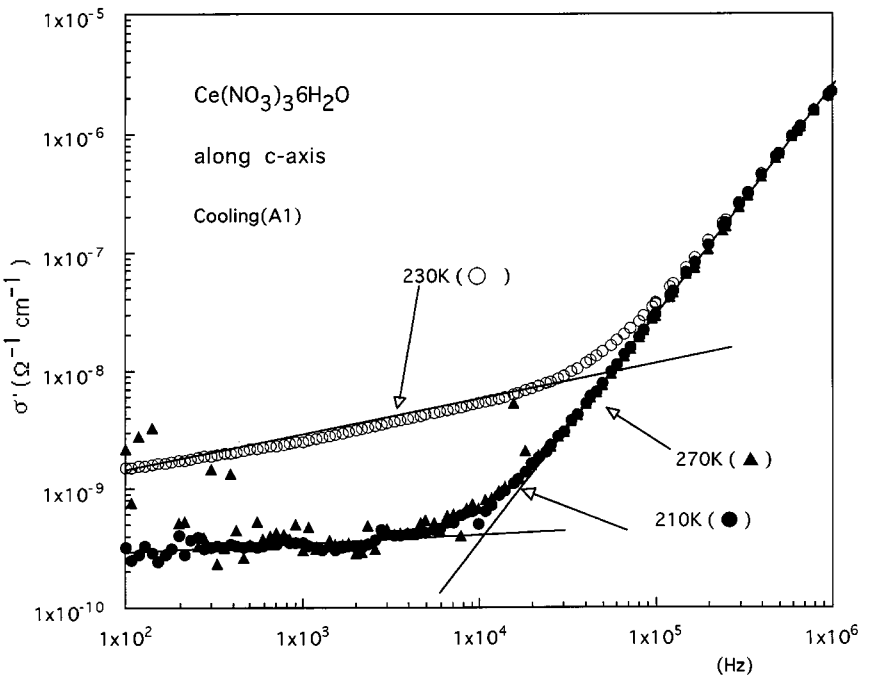

FIG. 2. Frequency variation of the real part σ' for the complexconductivity σ^* along the c axis at several temperatures in cooling (A1).

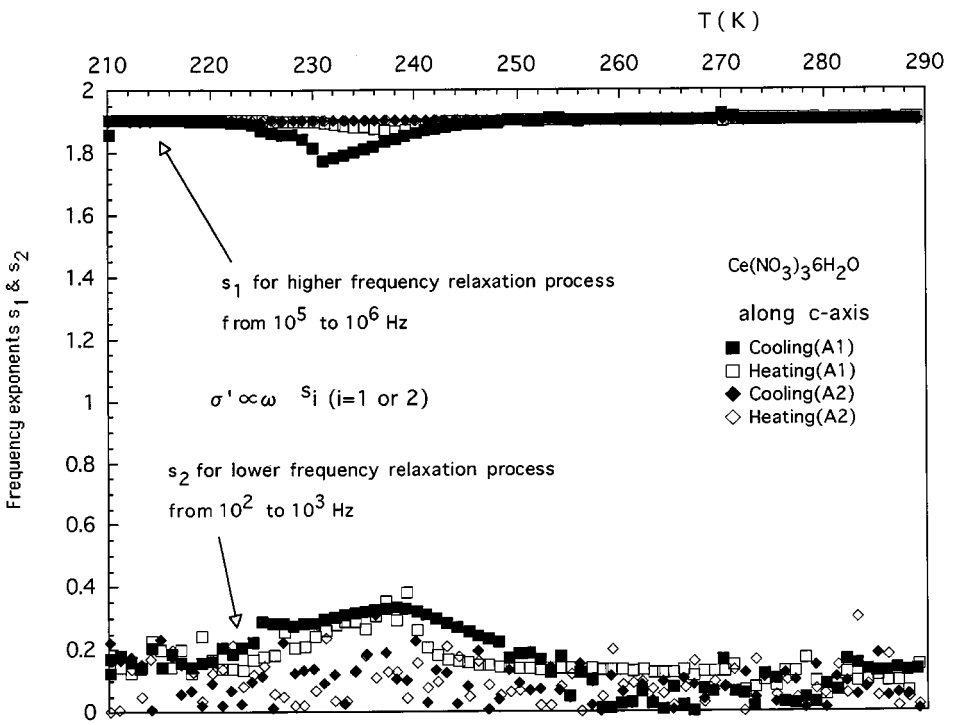

FIG. 3. Frequency exponents $s_1(T)$ and $s_2(T)$ to characterize the power law behavior of the ac conductivity spectra along the c axis of the $Ce(NO_3)_3 \cdot 6H_2O$ crystal in two frequency regions, $10^2 \sim 10^3$ Hz and $10^5 \sim 10^6$ Hz, respectively, at temperatures $210 \leq T \leq 290$ K in cooling (A1) (■) and (A2) (◆) and heating (A1) (□) and (A2) (◇) cycles of measuring runs.

perpendicular to the c axis. The $s_1(T)$ and $s_2(T)$ for the spectra $\sigma'(v)$ perpendicular to the c axis show a maximum near 145 K and a minimum near 125 K. The $s_1 \sim 1.95$ and $s_2 \sim 0$ along the c axis are temperature independent for $\sigma(v)$.

DISCUSSION

Static Property

Singularity in a temperature variation of a response function, such as ac conductivity, to an applied field in a crystal is attributed to anomalous fluctuation in the system accompanied with a phase transition phenomena(16). As seen from Figs. 1 and 5, $\sigma'(T)$ shows temperature variation in the higher temperature region, $243 < T < 293$ K, and the lower region near 130 K. Hence the phenomena in the higher temperature region results from a transition between a metastable and a stable phase occurring in a nonequilibrium manner. On the other hand, the singularity of $\sigma'(T)$, independent on the observation operation, in the lower temperature range is ascribed to the anomalous fluctuation in a normal transition phenomena.

However, $\sigma'(T)$ near the transition temperature regions shows the same dependence on the crystal direction, as given in Figs. 1 and 5. Additionally, the crystal structure is independent on temperature above 80 K (17). The transition phenomena in both temperature regions have the same mechanism and origin of the $Ce(NO_3)_3 \cdot 6H_2O$ crystal as that in the higher region and are sensitive to thermal effect.

The peak of $\sigma'(T)$ was observed in the lower temperature region, where a variation in the magnetic structure of Ce^{3+} was found by measuring the magnetization of the $Ce(NO_3)_3 \cdot 6H_2O$ crystal at temperatures between 4.2 and 300 K at 1 Tesla using the SQUID magnetometer (Quantum Design MPMS2). The anomalous fluctuation related to $\sigma'(T)$ in the temperature region is attributed to the characteristic electronic configuration of the ion in the crystal. The fluctuation in the electronic state of Ce^{3+} corresponds to valence one.

The dependence of the metastable phenomena on the rare-earth ion (isotope effect) (4–11) was observed in the higher temperature region.The origin of the transition phenomena is related to the valence fluctuation in the rare-earth ion R^{3+} in the crystal.

The crystal structure of $Ce(NO_3)_3 \cdot 6H_2O$ (18) at room temperature is composed of polyhedra with a high coordination number formed by the oxygen atoms of six-crystal water molecules and three nitrate ions. The rare-earth ion R^{3+} is caged in a high-coordination polyhedra (19) linked together by a hydrogen bonding network (20).

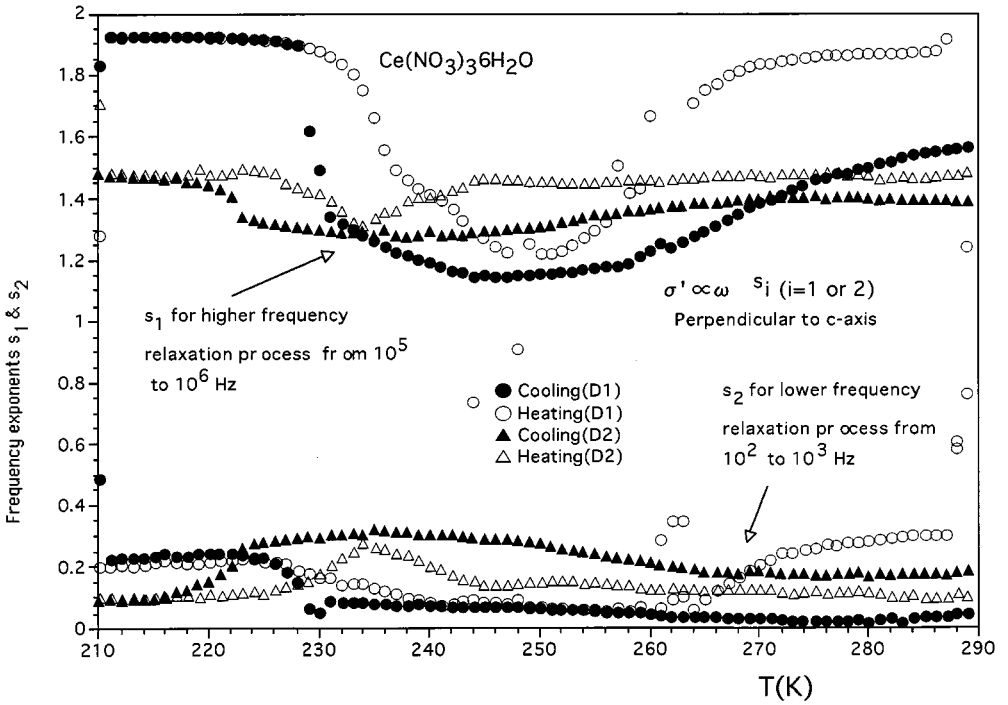

FIG. 4. Frequency exponents $s_1(T)$ and $s_2(T)$ to characterize the power law behavior of the ac conductivity spectra perpendicular to the c axis of $Ce(NO_3)_3 \cdot 6H_2O$ in two regions, $10^2 \sim 10^3$ Hz and $10^5 \sim 10^6$ Hz, respectively, at temperatures $210 \leq T \leq 290$ K in cooling (D1) (●) and (D2) (▲) and heating (D1) (○) and (D2) (△) cycles of measuring runs.

The high-coordination polyhedron plays an important role in the mechanism of the metastable phenomena. The valence fluctuation is attributed to nonequilibrium dynamics of the f electron having relatively large angular momentum in its inner atomic shell (2). The valence fluctuation is dependent on not only the material effect surrounding the rare-earth ion (1) but aslo the thermal effect.

The local fluctuation in complex polarization of the polyhedron caused by the valence fluctuation of the rare-earth ion R^{3+} inside it grows into a metastable disordered state in the crystal through the hydrogen bonding network, as seen in the transitions between ferroelectric and paraelectric phases of the potassium dihydrogen phosphate crystal (KH_2PO_4) (21).

Dynamical Property

The dynamical properties in these temperature regions are apparent in the ac conductivity (see Figs. 1–6).

Ac conductivity in the insulating material is attributed to a dielectric response to an altering electric field (22) and gives a time-dependent correlation function between the fluctuations in the crystal. The Debye model shows the dielectric response to the altering electric field of an isolated charge that can occupy one of two localized sites or equivalently an inertialess dipole that can assume one of only two spatial configurations. The Debye response is defined by the relaxation of the polarization obeying a first-order equation characterized by a single, fixed relaxation time τ (23). The spectra $\sigma'(\nu)$ can be expressed in terms of the dielectric loss $\varepsilon''(\nu)$ in the Debye response,

$$\sigma'(\nu) = \varepsilon_0 2\pi\nu\varepsilon''(\nu) = \frac{\varepsilon_0(2\pi\nu)^2\tau}{1 + (2\pi\nu)^2\tau^2} \qquad [2]$$

At low frequencies ($\nu \ll 1/\tau$), $\sigma'(\nu)$ can be approximated as $\sigma' \propto (2\pi\nu)^2$ ($s = 2$).

In amorphous semiconductors (and some other disordered systems), a frequency-dependent conductivity increases approximately linearly with frequency at least in the frequency range, $10 < \nu < 10^8$ s^{-1}, and the frequency exponent $s \leq 1$ (15).

The phenomenon has been ascribed to relaxation caused by the motion of electrons, or atoms, hopping or tunnelling between equilibrium sites. In the case of the random systems, and noncrystalline materials, relaxation occurs due to processes involving distances or activation energies intimately related to the disordered structure of the materials, which themselves have a broad distribution of values. A

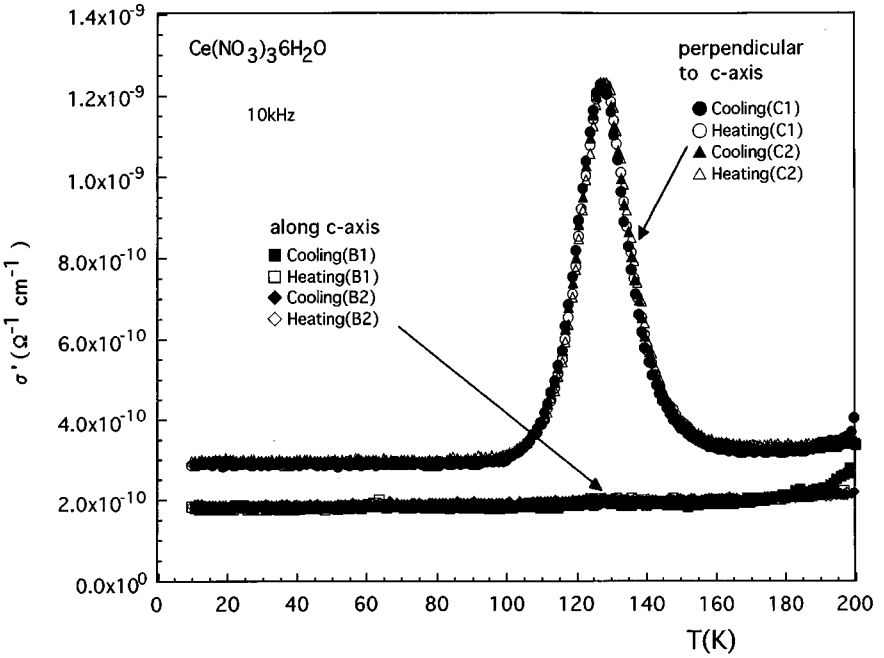

FIG. 5. The real part σ' of the complex conductivity σ^* at 10 kHz of the $Ce(NO_3)_3 \cdot 6H_2O$ crystal at temperatures T between 200 and 10 K, along the c axis in cooling (B1) (■) and (B2) (◆) and heating (B1) (□) and (B2) (◇) cycles of double measuring runs and perpendicular to it in cooling (C1) (●) and (C2) (▲) and heating (C1) (○) and (C2) (△) cycles of double measuring runs.

distribution of the relaxation times exist. For a continued distribution of $n(\tau)$, $\sigma'(\nu)$ can be written as

$$\sigma'(\nu) = \int_0^\infty \alpha n(\tau) \frac{(2\pi\nu)^2\tau}{1 + (2\pi\nu)^2\tau^2}\, d\tau, \qquad [3]$$

where α is the polarizability of a pair of sites, for the moment assumed to be independent of τ (after (15)). The linear frequency dependence observed in amorphous semiconductors can be obtained from Eq. (3) for $n(\tau) \propto 1/\tau$.

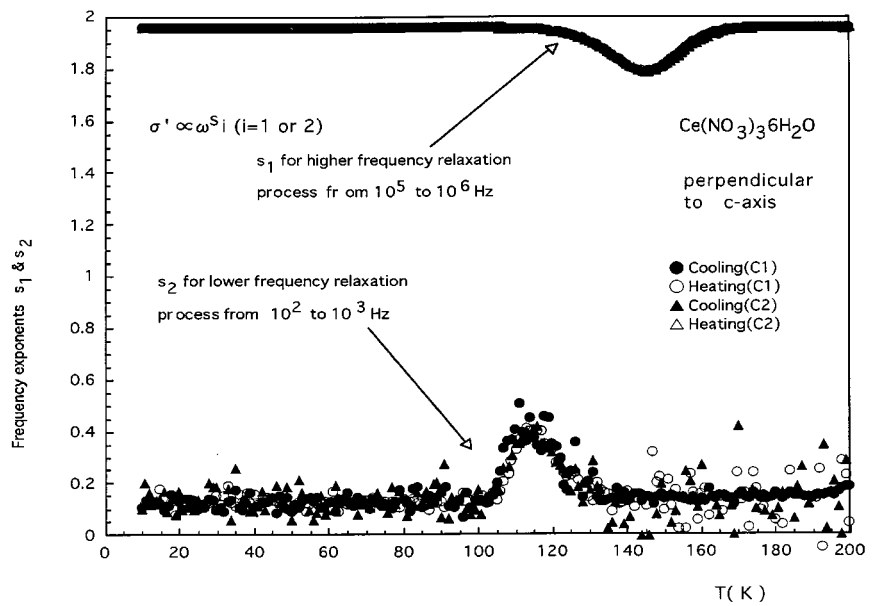

FIG. 6. Frequency exponents $s_1(T)$ and $s_2(T)$ to characterize the power law behavior of the ac conductivity spectra perpendicular to the c axis of $Ce(NO_3)_3 \cdot 6H_2O$ in two regions, $10^2 \sim 10^3$ Hz and $10^5 \sim 10^6$ Hz, respectively, at temperatures $10 \leq T \leq 200$ K in cooling (C1) (●) and (C2) (▲) and heating (C1) (○) and (C2) (△) cycles of measuring runs.

As seen in Figs. 3, 4, and 6, the value of s_1 for the higher frequency region, $10^5 \leq \nu \leq 10^6$ Hz, is nearly equal to 2.0 for the spectra $\sigma'(\nu)$ along the c axis and perpendicular to it, except for the temperature regions of the metastable phase and those assigned to the Debye response. On the other hand, as found in these figures, the values of s_2 for the lower frequency response, $10^2 \leq \nu \leq 10^3$ Hz, are below 1.0, and hence the dispersion in the lower frequency region would be similar to those observed in the disordered system. The ac conductivity spectra in the two frequency regions can be assigned to different dynamical processes.

The anomalous temperature dependence (minima of s_1 and peaks of s_2) of the frequency exponents are found in Figs. 3 and 4 for the higher temperature region and in Fig. 6 for the lower region at the transition temperatures. These singularities of $s_i(T)$ $(i = 1,2)$ suggest the variation in the relaxation processes of the fluctuation in the crystal.

Summary

The transition phenomena in the present study have nonequilibrium higher topological order and are related to the valence fluctuation induced in the crystal. The fluctuation is nonergodic and nonlinear, and hence to clarify the property of the transition phenomena it is not sufficient to base measurements on average behavior of the crystal but on the time series behavior (24). Additionally, the characteristic property of the rare-earth nitrate crystal is related to quantum chaos(25).

The structural model for the metastable phase in the rare-earth nitrate crystal refers to nonequilibrium behavior due to the frustration expected in the three-dimensional sphere packing of polyhedra or icosahedral bond orientation order in liquid, glass, or quasi-crystal (26).

Knowledge of both the more detailed mechanism and the more obvious origin for the transition phenomena is needed in order to apply information supplied by microscopic measurements, such as X-ray diffraction measurements in the rare-earth nitrate crystals at different temperatures.

REFERENCES

1. P. Wachter and H. Boppart (Eds.), "Valence Instabilities," North-Holland, Amsterdam, 1982.
2. Y. Onuki, K. Ueda, and T. Komatsibara (Eds.), Heavy Electron System, selected papers in physics, *J. Phys. Soc. Jpn.* (1994).
3. K. A. Gshneider Jr. and L. Eyring (Eds.), "Handbook on the Physics and Chemistry of Rare Earths", Vol. 8, pp. 302–334. North-Holland, Amsterdam, 1986.
4. R. Kawashima, T. Saitoh, and H. Isoda, *J. Phys. Soc. Jpn.* **62,** 4529 (1993).
5. R. Kawashima, M. Hattori, and H. Isoda, *J. Phys. Chem. Solids* **55,** 1331 (1994).
6. R. Kawashima and Y. Matsuda, *J. Phys. Soc. Jpn.* **59,** 3727 (1990).
7. R. Kawashima, T. Sasaki, and H. Isoda, *J. Phys. Soc. Jpn.* **63,** 2008 (1994).
8. R. Kawashima and H. Isoda, *J. Phys. Soc. Jpn.* **59,** (1990) 3408.
9. R. Kawashima, S. Nasukawa, and H. Isoda, *J. Phys. Soc. Jpn.* **64,** 1439 (1995).
10. R. Kawashima, *J. Phys. Soc. Jpn.* **60,** 342 (1991).
11. R. Kawashima, R. Takahashi, and H. Isoda, *J. Solid State Chem.* **121,** 74 (1996).
12. R. Kawashima, and collaborators, *Physica B* **183,** 135 (1993); *Physica B* **203,** 59 (1994); *J. Phys. Chem. Solid* **57,** 539 (1996); *CHAOS* **7,** 1863 (1996).
13. R. Kawashima and H. Isoda, *Phys. Status Solidi A* **145,** K59 (1994); **153,** 501 (1996); *J. Phys. Soc. Jpn.* **64,** 684 (1995); **65** 1133 (1996).
14. "Gmelin Handbuch der Anorganischen Chemie, System," No. 39. Springer-Verlag, Berlin/New York, 1974.
15. R. Elliott, *Adv. Phys.* **36,** 135 (1987).
16. H. E. Stanley, "Introduction to Phase Transitions and Critical-Phenomena." Clarendon Press, Oxford, 1971.
17. R. Kawashima, M. Sasaki, S. Satoh, H. Isoda, Y. Kino, and Y. Shiozaki, to be published.
18. N. Milinski, B. Ribar, and M. Sataric, *Cryst. Struct. Comm.* **9,** 473 (1980).
19. E. L. Muetterties and C. M. Wright, *Q. Rev. Chem. Soc.* **21,** 109 (1967).
20. G. C. Pimentel and A. L. McClellan, "The Hydrogen Bond," pp. 255–295. Freeman, San Francisco, 1960.
21. M. E. Lines and A. M. Glass, "Ferroelectrics and Related Materials," pp. 293–321. Oxford Univ. Press, London, 1977.
22. A. K. Jonscher, "Universal Relaxation Law." Chelsea Dielectric Press, London, 1996.
23. V. V. Daniel, "Dielectric Relaxation," Ch. 2, pp. 13–31. Academic Press, London, 1967.
24. R. Kawashima, R. Hattada, and H. Isoda, *J. Phys. Soc. Jpn.* **68**(4), in press (1999).
25. K. J. Strandburg (Ed.), "Bond-Orientational Order in Condensed Matter Systems," pp. 137–211 and 255–281. Springer-Verlag, Berlin, 1992.
26. T. Dittrich, P. Hänggi, G.-L. Ingold, B. Kramer, G. Schön, and W. Zwerger, "Quantum Transport and Dissipation." Weily–VCH, Weinheim, 1998.